Evaluation of epigenetic drug targeting of heterogenous tumor cell fractions using potential biomarkers of response in ovarian cancer

Anand Kamal Singh [1], Nishi Chandra, Sharmila A. Bapat[1,2]

[1]National Centre for Cell Science, NCCS Complex, Pune 411007, INDIA
[2]Corresponding author: Sharmila A. Bapat, National Centre for Cell Science, NCCS Complex, Pune 411007, INDIA, Tel.91-020-25708074, email:sabapat@nccs.res.in

Running Title: Biomarkers of response for epigenetic drug evaluation

Keywords: Epithelial ovarian cancer, DNA methylation, Histone methylation, Epigenetic drugs; Intratumor heterogeneity; biomarkers of response

Translational Relevance

Epigenetic gene dysregulation is associated with tumor formation and progression to a malignant stage. In the present study, altered DNA and histone methylations along with expression profiles of an *in vitro* progression model of serous ovarian cancer were compared with those in tumors to derive a panel of candidate biomarkers. Three of these markers *viz.* PTGIS, MEST and RXRγ were further profiled across heterogeneous cell fractions in tumors to predict possible tumor recurrence following treatment with either 5-Aza-dC, Trichostatin A, Curcumin or CBB1007. Such evaluation of drug efficiencies has different long-term regenerative implications, since it not only assigns predictive potential to candidate biomarkers in response to treatment, but also indicates the tumor cell population likely to be refractory to treatment

Abstract

Purpose: Resolution of aberrant epigenetic changes leading to altered gene expression during transformation and tumor progression is pertinent for mechanistic understanding of disrupted pathways in cancer. Such changes provide for biomarkers that can be applied in drug screening and improved disease management.

Experimental Design: Genome-wide profiling and analyses of promoter DNA methylation, histone modifications and gene expression of an *in vitro* progression model of serous ovarian adenocarcinoma were carried out. Similar *in silico* analyses and comparison of methylation and gene expression of early and late grade ovarian cancer samples in The Cancer Genome Atlas assigned a clinical relevance to our study. Candidate biomarkers were evaluated for epigenetic drug treatments in experimental animal models on a background of differing tumor cell responses arising from intra-tumor heterogeneity.

Results: Differentially regulated genes during tumor progression were identified through the above analyses as candidate biomarkers. In examining the tumor suppressor PTGIS as a potential biomarker for treatment with either 5-Aza-dC or TSA , 5-Aza-dC effectively stabilized cell cyling, restricted genetic instability and derepressed *PTGIS* expression, while TSA led to emergence of drug resistant progenitors lacking PTGIS expression. Profiling MEST and RXRγ for Curcumin and CBB1007 respectively indicated an inability of Curcumin and CBB1007 in restricting residual tumor regenerative capabilities.

Conclusions: Our study provides novel insights into epigenetic regulation in ovarian cancer progression and potential biomarkers for evaluating efficacy of epigenetic drugs in restricting residual tumor regeneration. Such approaches may assign a new functional interpretation of drug efficacy and cell tumor responses in ovarian cancer.

Introduction

Genetic and epigenetic changes disrupt gene expression and molecular behavior of normal cells, driving them towards transformation (1, 2). Methylation of cytosine residues in CpG islands within gene promoter regions directly regulates transcription by inhibiting binding of specific transcription factors to the DNA; while indirect regulation through recruitment of repressive chromatin-remodeling methyl-CpG-binding proteins is reported (3-7). Besides DNA methylation, histone modifications, particularly tri-methylation of histone 3 tails at lysines 4, 9 or 27 [H3K4me3 (K4), H3K9me3 (K9), H3K27me3 (K27) respectively] are extensively studied in the context of transcriptional regulation (8-11). Definitive roles for histone methyltransferases and histone acetyltransfearses as “writer” and histone demethylases and deacetylases as “eraser” molecules in tumor initiation and progression further confirm the involvement of methylated histones in cancer (12-14).

Epigenetic alterations being less rigid than genetic changes hold the promise of possible treatment avenue in different tumor types by rendering tumor cells responsive to drugs through reversal of aberrant ‘epigenetic marks’ (15). Ovarian cancer, the most lethal amongst gynecological malignancies is associated with late diagnosis, rapidly advancing disease and frequent, aggressive post-therapeutic recurrence (16,17). Altered CpG methylation, identified as an early event in epithelial ovarian cancer pathogenesis (18-22) complements histone methylations in modulating biological functions in the disease (23,24). In the present study, we studied these epigenetic mechanisms in correlation with altered gene expression in an *in vitro* progression model of serous epithelial ovarian cancer (25). Further, to explore the clinical relevance of our findings, we concurrently analysed methylation and expression data of serous ovarian tumors available with The Cancer Genome Atlas (TCGA; 6;http://tcga-data.nci.nih.gov/tcga/dataAccessMatrix.htm). These consolidated efforts identified a subset of epigenetic biomarkers associated with ovarian cancer transformation and progression. We further evaluated the suitability of these biomarkers in predicting *in vivo* tumor responses to four epigenetic drugs through resolution of discrete cellular fractions within xenografts (27; 28). Together, our findings present a novel and comprehensive approach for the derivation of potentially predictive biomarkers that provide a read-out for evaluating epigenetic drug efficacy and tumor responses for development of next-generation generation drugs in serous ovarian adenocarcinoma.

Materials and Methods

Cells, culture and xenograft generation: A4, a serous ovarian adenocarcinoma cell line established in our lab (25), was derived as a non-tumorigenic single cell clone isolated from patient tumor ascites that underwent spontaneous transformation. These paired cells considered as representative of pre-transformed and transformed cellular states (A4-P and A4-T respectively;29), were maintained in MEM medium+5% fetal bovine serum+1% nonessential amino acids and grown at 37°C, 5%CO_2 in humidified atmosphere. PKH26 / PKH67 (Sigma) labeling of cells is described earlier (27). 2.5×10^6 A4-T cells were used for generating subcutaneous (s.c) xenografts in 8-wk non-obese diabetic/severe combined immunodeficiency mice maintained under sterile airflow conditions. All experimental animal procedures were done in accordance with NCCS Institutional Animal Ethics Committee clearances, laws, and policies; animals were monitored every alternate day after cell injection. Harvested tumors were measured, processed for digestion and other studies; Tumor Volume = Lengthx ($Width^2$)/2 cm^3 (30).

Methylated DNA immunoprecipitation (MeDIP), Chromatin immunoprecipitation (ChIP), Promoter array, Transcriptome analyses and Correlation between Methylation and Expression Data: MeDIP/ChIP was performed with fragmented (300–1000bp) genomic DNA from sonicated A4-P or A4-T cells. For immunoprecipitation, 4mg of sonicated DNA was incubated for 12 h at 4°C with anti-5-methylcytosine/K4/K9/K27 monoclonal antibody; standard protocols were followed for further enrichment and hybridization (31). Genome wide promoter methylation profiling was performed using Agilent Human Promoter CpG 244k Array (G4492A); Agilent Human Promoter CoC 244k (G4489A) was used for histone methylation (31). MeDIP-chip (promoter DNA methylation) or ChIP-on-chip (histone methylation) data analysis was performed with Agilent genomic workbench. Pre-processing and initial analysis was done by applying Whitehead neighbourhood error model algorithm in Agilent DNA analytics. Data from each array was subjected to Median Blanks subtraction, inter-array median normalization and dye-bias median normalization. Probe distribution on arrays to identify regions of increased / probe signals/peaks were extracted and collapsed with GSEA (Gene Set Enrichment Analysis; 32) to obtain negatively and positively enriched probes (enrichment ratios < -1 and > +1 respectively; $p<0.05$). For DNA methylation datsets, negatively enriched probes were considered as hypomethylated while positively enriched probes were considered as hypermethylated genes.

Gene expression profiles of A4-P and A4-T cells submitted earlier as GSE18054 were subjected to univariate analysis for class comparison as described earlier ($p<0.01$; 33). TCGA ovarian cancer samples were segregated into two groups, wherein Group1 comprised of Grade1 and Grade2 samples (n=6, n=69 respectively) that were comparable to A4P, while Group2 consisting of Grade 3 samples (n=484) were compared with A4T. Datasets of these tumors were subjected to class comparison with univariate test for probes with p-value <0.01; analysis was done using BRB array tools (for collation and median deviation analyses); Perl programming further used to identify hypomethylated and hypermethylated genes (β-values < 0.3 and > 0.7 respectively; 34). A flow-chart of the outcome of this derivation is represented in Supplementary Fig.1. Correlation between DNA methylation and gene expression was visualized as Starburst plots. Briefly, p-values of differential genes for methylation and expression in three different datasets *viz.* A4, Group1 TCGA and Group2 TCGA were determined by Bonferroni correction before applying a false discovery rate (FDR) adjustment across all probes for pair wise comparison (FDR adjusted to p-value <0.05; Benjamini and Hochberg method was used (35).

Bisulfite genomic sequencing (BGS): Bisulfite modification of 500ng-1µg genomic DNA from A4P and A4T cells was achieved using EpiTect Bisulfite Kit (Qiagen). Probes for BGS were designed around differentially enriched CpG islands identified through MeDIP using Methprimer software (36). PCR products generated from amplification of bisulfite modified DNA were purified by using QiaQuick Gel Extraction Kit (Qiagen) and cloned into pGMT easy vector (Promega). Blue-white screening and selection of at least 10 clones followed transformation; clones were sequenced by Big Dye Terminator method and analyzed for CpG methylation using BiQ Analyzer software (37). Methylation index (MI) was calculated as –

$$MI = \frac{\text{Number of methylated CpGs}}{\text{Total number of CpGs}} \times 100$$

Drug dosage and administration: Standard MTT assays were performed to identify IC_{50} doses of 5Aza-dC, TSA, Curcumin and LSD1i (5/3/3/7µM respectively at 48 hours) for A4T cells; these drug concentrations were used in the *in vitro* functional assays. For *in vivo* studies drugs were administered 15 days after initiation of A4 subcutaneous xenografts at tumour site in NOD-SCID mice (n=3 for each treatment and control) at a final drug concentration of 5/3/3/7 mg/kg of body weight (5Aza-dC, TSA, Curcumin and

LSD1i respectively). Drug regime comprised of administration on three alternate days followed by one week recovery before tumors were harvested for analysis (detailed regimes described in Supplementary Fig.4d).

RNA extraction, cDNA preparation, RT-PCR, quantitative PCR (q-PCR), ChIP-qPCR: RNA extraction, cDNA preparation and amplification from cells and tumors were performed as described earlier (29). Amplified products were run on 1.5% Agarose gel; ß-Actin was used as the internal control in all reactions. Each gene expression was normalized with corresponding β-actin expression in the sample and fold-changes estimated vs. control samples. Gel images were captured on a SYNGENE gel doc system at 3msec UV exposure and converted into JPEG format without post processing. Densitometry analysis was carried out with gel analyses software GENETOOL. qPCR analyses with specific gene primers were carried out with Step one plus in 96-well plate format using SYBR Green Mix (Life Technologies). Changes in threshold cycle (C_T) values were calculated as : $\Delta C_T = C_T$ (test) - C_T (control); fold difference was calculated as: fold difference= $2^{-\Delta(\Delta C_T)}$. Actin expression was used for normalization; non-template controls accounted for possible contaminating DNA in reaction mixtures. ChIP-PCRs were performed as per standard protocols using K4/K9/K27 antibodies and primers flanking enriched probes; specific primer sequences for all amplifications can be provided on request.

Apoptosis assays, FACS staining and resolution of various tumor cell fractions: Annexin V–FITC based apoptosis was assayed as described earlier (38) and acquisitions were made on FACS Canto II; DiVa software (Becton Dickinson) was used for data analysis. For analysis of heterogeneous populations, unlabeled tumor cells were used as controls for gating total dye quenching events, while freshly labeled cells were used as positive controls. Propidium idodide (PI), Hoechst–PyroninY staining was carried out as described (28).

Clonogenecity (Adherent / non-adherent / Soft Agar Colony), spheroid formation, wound healing assays and Immunostaining: 5×10^2 sorted tumor cells were added per well in 96-well culture plates. After incubation at 37°C for 14 days, cells were washed twice with PBS and stained with 0.05% crystal violet in 20% methanol. For soft agar assays, 5×10^3 sorted tumor cells were suspended in 0.5% low melting agarose (Sigma) in 2xMEM, plated above a layer of 1% agarose in 35mm dish, incubated at standard

conditions for 3 weeks, colonies stained with 0.005% crystal violet. Adherent and non-adherent colonies were photographed and counted with Image J software (NIH, USA). For generating tumor spheroids, $5x10^4$ sorted tumor cells were plated per well in 24-well ultra-low attachment plates in MEM+1% FBS. Developing spheroids were counted at Days 6, 9 and 12 (20x; inverted phase contrast microscope). For wound healing/ cell migration, 96 well plates were seeded with 1000 sorted tumor cells/ well, media changed every alternate day and cells allowed to grow till 90% confluency. Wound was inflicted with a pipette tip, two washes with 1XPBS followed to remove floating cells and media (lacking serum) was added. Migration was monitored for 72 hours; images captured on Olympus IX71 microscope and analysed by TScratch Software. For Immunostaining, adherent cells/spheroids were washed with 1XPBS, fixed with 4% paraformaldehyde, membranes permeabilized with 0.01% Triton X-100. Following blocking with 5% goat serum in phosphate-buffered saline (PBS), primary antibody (Sigma) was added (30 minutes, ambient temperature), followed with secondary Alexa 488-labeled antibody (Invitrogen) for 20 minutes; Hoechst (Sigma-Aldrich) was used for nuclear counterstaining and confocal images were captured (63x Carl Ziess).

Statistical analyses: Unless mentioned otherwise, all experiments were done in triplicates and data represented as Mean $\pm$ standard deviation (Sigma Stat software). Paired t-test was performed to determine significant differences between the groups.

Results

Genome-wide DNA methylation and expression analyses of the progression model and correlation with corresponding datasets and tumor TCGA groups

Whitehead pre-array neighborhood model based analysis (threshold at $p<0.05$) of the A4 progression promoter methylation data associated 13,786 and 2253 genes with A4P and A4T respectively. Differential enrichment analysis ($+1 \leq$ enrichment ratios ≤ 1) further revealed 2395 positively and 1159 negatively enriched (hyper- and hypo-methylated) genes in A4-P cells, and 257 hyper- and 559 hypo-methylated genes in A4-T cells. This correlates with 137 genes that undergo promoter hypomethylation while 32 genes undergo promoter hypermethylation during progression from a pre-transformed to transformed state (Fig.1a-i; Supplementary Fig.2a). Similar class comparison of gene

expression data revealed 1764 differentially expressed genes (957 up- and 807 down-regulated respectively) during this progression (Supplementary Fig.2b). Correlations between methylation and expression identified 76 hypo-methylated - upregulated genes, and 31 hypermethylated - downregulated genes during A4 progression (Fig.1a-ii; Supplementary Table 1).

To probe for clinical relevance of these genes during disease progression, we similarly analyzed DNA methylation and expression datasets of 559 TCGA ovarian adenocarcinoma samples that were segregated as Group1 (Grades I & II) and Group2 (Grade III;Methods). This identified 5776 hypo- and 621 hyper-methylated genes for Group1 tumors of which 1536 and 155 were up- and down-regulated respectively at the expression level; while of the 4294 hypo- and 147 hyper-methylated genes in Group2 tumors, 2028 and 54 genes were up- and down-regulated respectively (Figs.1b-i;1b-ii; Supplementary Fig.2c). Higher negative enrichment suggests promoter hypomethylation rather than hypermethylation as being significant in ovarian tumor progression. Overlapping the A4 and TCGA datasets further identified a common association of 5 hypo- and 3 hyper-methylated genes with pre-transformed/early grade, and 15 hypo- and 2 hyper-methylated genes with transformation and malignant high-grade disease (Figs.1c-i,ii;1d-,d-ii;Supplementary Fig.1). Functional annotation of these genes assigned cell component morphogenesis, regulation of cell proliferation and/or apoptosis with neuronal development as being important during transformation and tumor progression (Supplementary Fig.2d). Of these strongly associated genes, we had earlier identified *MAL, MEST, FBN1, PAPSS2* and *PTGIS* as components of a SeOvCa gene expression signature (31).

Validation of differentially methylated genes in the progression model

Bisulfite genomic sequencing (BGS) based validation of the signature genes along with differentially methylated *CYC1* and *POGK* ($p<0.05$) affirmed demethylation of *CYC1, POGK, MAL* and *MEST* ($p\leq0.01$;2~4–fold decrease in MI;Figs.2a,2b) and methylation of *PAPSS2* and *PTGIS* ($p\leq0.05$; >1.5 fold increase in MI) during progression. Although methylation status of the Ci CpG (-247 to -700bp) island in *FBN1* promoter could not be validated, two other CpG islands *viz.* Cii (-731 to -1051) and Ciii (-1287 to -1645) were indeed differentially methylated (Fig.2a). Associations of differential promoter methylation and expression of these genes were also affirmed; thus hypomethylated *CYC1, MAL,*

MEST and POGK were expressed, while hypermethylated *FBN1 and PTGIS* were repressed (p≤ 0.01; 2~10 fold increased/decreased expression respectively;Figs.2c-i,2c-ii). Effectively, convincing correlations between CpG methylation and expression during progression were identified.

Genome-wide histone methylation analyses and correlation with gene expression during progression identifies additional epigenetic markers

Genome-wide histone methylation profiles (K4,K9,K27) during A4 progression established through ChIP-on-chip (CoC) were analyzed to identify gene promoters differentially enriched with histone marks based on probe specificity and enrichment ratios (p≤0.05; ER>1). Transformation was associated with maximum enrichment of monovalent K4 followed by K27 and K9 methylation; bivalent K4-K9, K9-K27, K4-K27 and trivalent K4-K9-K27 marks were also significantly enriched (Fig.3a;Supplementary Table 2). Functional association of specific histone marks with gene expression was identified, whereby K4 enriched genes were expressed at high levels, those with K9 or K27 marks at low levels, bivalent K4-K9 or K4-K27 marks at moderate to high levels, while genes carrying bivalent K9-K27 (22) or trivalent K4-K9-K27 (39) marks were repressed (Fig.3b; Supplementary Table 3).

To validate the exclusive functional effects of histone methylation on gene expression distinct from those of DNA methylation, twenty-three differentially regulated genes that did not exhibit methylated promoters but exclusively harbored histone marks in the progression model as well as TCGA cohort (Supplementary Table 4) were profiled for differential expression (Fig.3c;Supplementary Fig.3a). Six of these genes did not follow the histone code in both datasets. K4-associated upregulated genes included *HDAC2, SIN3A, MBD1, RRM2, UTX*; *PAX2* was downregulated by K9, *NCRA* by K9-K27 and *ASCL2* by K4-K9-K27 marks. Differential expression of *HOXA1* and *EMD* were not indicated in tumor grade progression while anti-correlative differential expression of *RXRγ, IL4, NCR2*, *UTX*, *WNT8B, SMARCA2, HOXB7* between the two models under study *viz.* A4 and TCGA tumor grade progression indicated discordance between *in vitro* and clinical data as is often reported.

Further functional validation of such associations between histone marks and gene expression in the progression model revealed a variance from the CoC-based identification (Figs.3d,3e). Of the K4 targeted genes, *MBD1* and *HDAC2* affirmed the

association, while in *SIN3A, RRM2* and *UTX*, promoter activation and gene expression is additionally associated with reduced K9 and/or K27 marks in transformed cells. Likewise, both monovalent K9 gene promoters *viz. HOXA1* and *PAX2* additionally acquired K27 marks and lost K4 marks to correlate with decreased expression. Of the K27 associated genes, *WNT8b* exhibited an additional K9 mark leading to bivalent repressive regulation; *RXRγ* promoter acquired K27 with loss of K4 and K9 marks, while contrary to CoC prediction the *IL4* promoter lost K4 and K27 but acquired a K9 mark. Similarly, multivalent marks were affirmed through specific histone affinities and expression for *EMD* (K4-K9), *CYP26B1* (K4-K27) and *ASCL2* (K4-K9-K27) promoters; a weak association of (K9-K27) was evident at the *NCR2* promoter (Fig.3d). Cell function based annotation of these genes identified altered metabolism, transcriptional regulation and cellular biosynthesis during transformation (Supplementary Fig.3b).

Interestingly, progression was associated with increased DNA hypomethylation and activating histone marks that suggests a high transcriptional turnover during transformation. An important functional correlation relevant in this context emerged as activation of the transcriptional repressor machinery (*SIN3A, MBD1, HDAC2*) through association with a K4 mark. Other novel observations include repression of differentiation and immuno-responsive genes (*HOXA1*,*WNT8b*,*RXRγ*,*IL4*) that could alter the kinetics of tumor regeneration during progression by generating differentiation arrested progenitors and apoptosis-resistant tumor cells. In an earlier proteomics-based study, we identified *RXRγ* downregulation as a key feature in acquisition of resistance to apoptosis during transformation (29). Importantly, the present finding suggesting this repression to be mediated by a K27 mark assigns dysregulation at the epigenetic level, and provides an opportunity to re-sensitize tumor cells with epigenetic drugs. Collectively, this data assigns importance to acquired DNA and histone methylation in regulating cellular pathways during disease progression.

Epigenetic drugs restrict ovarian cancer growth with each drug exhibiting differential targeting of discrete tumor cell populations

Exposure of the progression model to four epigenetic drugs including 5-Aza-dC, Trichostatin A (TSA), curcumin and a novel LSD1 inhibitor CBB1007 (LSD1i;Merck-Millipore) strikingly showed more rapid and pronouncedapoptotic effects in A4T than A4P cells (Figs.4a; Supplementary Fig.4a). All drugs were cytotoxic; curcumin and TSA

aggressively induced late apoptosis (Annexin V+/PI+) as compared to 5-Aza-dC and LSDi that induced a higher frequency of early apoptosis (Annexin V+/PI-) indicating a latency in drug action. We also evaluated residual regenerative potential by evaluating tumor spheroid forming capability of A4T cells following each treatment (Supplementary Fig.4b). This indicated that while all drugs effectively targeted this self-renewal capability, TSA and curcumin were more efficient than 5-Aza-dC and CBB1007. Further, assessment of *in vivo* drug effects on A4T xenografts mice subjected to defined regimes indicated significant tumor regression with each of these drugs (Supplementary Fig.4c).

Towards a mechanistic understanding of drug cytotoxicity, we delineated the specific cellular targets of each drug vis-à-vis discrete cellular subsets resolved through flow cytometry based on the cancer stem cell (CSC) hierarchy, genetically unstable populations (aneuploidy) within xenografts and differential cell cycling as described earlier (28). Briefly, label-chase of vital membrane dyes (PKH26/PKH67) resolves the CSC hierarchy as three cell subsets with a decreasing order of regenerative potential *viz.* PKH^{hi} cells (quiescent CSCs), PKH^{lo} (progenitors) and PKH^{neg} (host and differentiated tumor cells; Supplementary Fig.4d-Level1). Another parameter defined is genetic instability, established through DNA content profiling with propidium iodide (PI) staining that demarcates euploid and aneuploid fractions within the xenograft (Supplementary Fig.4d-Level2). PI staining also quantifies cells in basic cell cycle phases (G0/G1,S,G2/M); supplementing this with combinatorial Hoechst-Pyronin Y staining (DNA and RNA content based analysis) further resolves G0 from G1 fractions (Supplementary Fig.4d-Level3).

All four epigenetic drugs significantly target the PKH^{neg} fraction (tumor bulk); this accounts for the tumor regression in response to drugs exposure (Fig.4b-left panels). Concurrent enrichment of regenerative PKH^{lo} and PKH^{hi} cells however suggests that these residual progenitors and CSCs may generate recurrent disease. Ploidy analyses revealed 5-Aza-dC and TSA treatments to effectively target the aneuploid fraction, while enhanced aneuploidy was evident post CB1007 treatment (Fig.4b-central panels). In comparing the effects on tumor cell cycle kinetics, 5-Aza-dC treatment exhibited elevated G0 levels (slower cell cycle progression with increased differentiation / dormancy), while CB1007 had opposite effects of reduced G0 with rapid cell cycling (Fig.4b-right panels). Enhanced S phase with cell cycling was observed following TSA or curcumin treatments. Importantly, such analysis that reveals a more incisive

understanding of drug effects and cellular targets indicated 5-Aza-dC to be most effective in restricting emergence of genetically unstable cells that are a likely source of drug resistance. We further tested the regenerative and invasive capabilities of the residual tumor cell fractions post 5-Aza-dC treatment that affirmed effective elimination of regenerative aneuploid cells in the residual tumors. While PKH^{hi} CSCs exhibited highest functional capabilities as assayed for formation of tumor spheroids, adherent and non-adherent colonies and cell migration, PKH^{lo} progenitors were not found lacking, and surprisingly few PKH^{neg} cells also acquired these capabilities (Figs.4c-i,c-ii,c-iii,c-iv;Supplementary Fig.5). Together, this suggests the re-establishment of a proliferative hierarchy that is refractory to 5-Aza-dC.

Integration of biomarker-drug associations along with resolution of tumor sub-populations is useful in prediction of long-term epigenetic drug efficacies

Functional assays associated all treatments with residual regenerative potential despite significant tumor regression. Towards an improved understanding, we queried the possibility of associating the epigenetic biomarkers as possible predictors of drug resistance / refractory behavior in specific tumor cell subpopulation(s) . The entire biomarker panel was thus profiled for altered expressions following drug treatment *in vitro* and *in vivo* to establish possible associations based on known mechanism of action (Fig.5a). 5-Aza-dC,TSA and CBB1007 treatments for DNA demethylation, histone deacetylase and LSD1 inhibition respectively would mediate de-repression, hence upregulated genes (fold-change$\geq$1.5) would qualify as optimal targets. Such an association established *PTGIS* as a marker for 5-Aza-dC as well as TSA (aberrant promoter and histone methylation); while a ~2.5 fold-change suggested *RXRγ* (aberrant K27 histone methylation) as a marker for CBB1007 treatment (Supplementary Fig.6a). Contrarily, evaluating curcumin for its role in inhibiting gene repression (through histone acetylation alone despite its range of other effects; fold-change$\leq$0.5), identified four putative markers *viz. MEST, SIN3A, RRM2* and *UTX*. Earlier reports of *MEST* as an ovarian cancer biomarker (aberrant demethylated promoter and loss of imprinting; 39) led to its selection in further detailed evaluation of drug action.

Thus, the frequency of tumor cells expressing *PTGIS* is enhanced following exposure to 5-Aza-dC as well as TSA, that for *MEST* is decreased on curcumin treatment, and *RXRγ* expression is elevated following CB1007 exposure (Figs.5a;Figs.6a-i,b-i; Supplementary

Author Manuscript Published OnlineFirst on June 30, 2015; DOI: 10.1158/1078-0432.CCR-15-0505
Author manuscripts have been peer reviewed and accepted for publication but have not yet been edited.

Fig.6b). Such profiling further introduced a complexity of molecular heterogeneity within the xenograft by identifying distinct fractions in which the marker is expressed (marker^{pos}) and those lacking marker expression (marker^{neg}). Towards complete understanding and assessment of drug efficacy *vis-à-vis* molecular as well as cellular tumor heterogeneity, we further delineated drug responses across the tumor regenerative hierarchy, genetic instability and differentially cycling cell populations not only over the entire xenograft, but also within the marker^{pos} and marker^{neg} fractions –

a. ***PTGIS* as a candidate marker for drugs targeting aberrant promoter and histone methylation -** 5-Aza-dC and TSA treatments led to significantly higher enrichment of CSCs and progenitors (PKH^{hi} and PKH^{lo} respectively) in the PTGIS^{pos} over the PTGIS^{neg} fraction. A major part of the PTGIS^{neg} fraction which constitutes most of the differentiated tumor bulk (PKH^{neg}) controls was drastically reduced (Fig.5c-i). Enhanced *PTGIS* expression was also evident in spheroids generated from residual PKH^{neg}, PKH^{lo} and PKH^{hi} cells Supplementary Fig.4c). Unfortunately, this suggests that other intrinsic drug resistant mechanisms may possibly shadow the tumor suppressor effects of *PTGIS*. Indeed, cell cycle analysis further revealed that while PTGIS^{pos} CSCs re-enter a cycling phase following both treatments, PTGIS^{neg} CSCs remain quiescent (Fig.5b-ii, Supplementary Fig.4d-i). 5-Aza-dC treatment however, resticts PKH^{lo} progenitor growth (G1-S growth arrest within PTGIS^{neg} fraction and quiescence in PTGIS^{pos} fraction, while no effects of TSA on progenitor cell cycling were evident. In evaluating the effects on emergence of genetic instability, PTGIS^{pos} euploid fractions were enhanced following on 5-Aza-dC/TSA treatments, while aneuploid fractions were diminished in the PTGIS^{neg} fraction (Fig.5d-i). Thereby, although both treatments effectively restrict genetic instability, cycling aneuploid cells in the PTGIS^{pos} fraction following TSA treatment (Fig.5c-ii) may further repopulate the tumor. 5-Aza-dC on the other hand, appears to effectively restrict frequency and cycling of aneuploid populations in either PTGIS^{pos} or PTGIS^{neg} fractions.

b. **MEST as a candidate marker for drugs targeting hypomethylation and/or LOI** – A majority of MEST^{pos} cells throughout the regenerative hierarchy were eliminated following curcumin treatment that reflected on decreased *MEST* expression in the entire tumor. MEST^{pos} CSCs were arrested in G1S phase, however MEST^{neg} CSCs and progenitors were significantly enriched and in a

cycling state (Fig.6a-ii,a-iii,a-iv,a-v), while other cells were in G0 phase (Supplementary Fig.6d-ii).

c. **RXRγ as a candidate marker for drugs targeting histone methylation -** CB1007 treatment led to upregulated RXRγ expression in A4T cells as well as xenografts (Fig.6b-i). This enriched expression resulted from drastically reduced $RXRy^{neg}$ differentiated cells and concurrent increase in $RXRγ^{pos}$ CSCs and progenitors. Despite their enrichment, a significant fraction of $RXRy^{neg}$ progenitors was in G0 (Fig.6b-ii;Supplementary Fig.6d-iii). The entire $RXRγ^{pos}$ fraction as well as $RXRy^{neg}$ CSCs and progenitors appeared to be cycling that possibly triggers genetic instability (Figs.6b-iii;6b-iv). Most aneuploid cells were however arrested in the G1S phase (Fig.6b-v).

Discussion

The stealth of epithelial ovarian cancer progression to an aggressive, drug-resistant disease has rendered it to be a 'silent killer'. In the present study we identified epigenetic dysregulation of cellular functions that complement aberrant gene and protein expression patterns in our experimental model that recapitulates disease progression (25, 29, 31, 40). Querying the clinical relevance of these epigenetic changes with tumors in the TCGA database revealed a small number of biomarker genes potentially associated with transformation (41-44; Box1, Level I). Thereby, reversal of the expression patterns of these genes could aid in predicting tumor cell responses to epigenetic drugs during ovarian cancer treatment (Box1-Level II).

Predictive biomarkers represent specific biologic characteristics that demarcate patient subpopulation(s) likely to benefit from a given therapy (45). Several studies demonstrating stabilization of expression patterns in response to epigenetic drug treatments remain limited due to lack of complete evaluation/prediction of long-term clinical responses (46,47). Importantly, intratumoral heterogeneity and minimal residual disease (MRD) are almost never considered in such studies and can become major deterrents in achieving drug efficacy (27,28,48). This realization led us to critically dissect out drug responses not only in terms of reversal of putative epigenetic biomarker expression patterns, but also evaluate functional associations *vis-à-vis* specific targeting of discrete tumor cell fractions as resolved through differential regenerative potential and

genetic instability. Further examining biomarker associations, stability of their expression, cell cycling and regenerative potential in residual tumor fractions established important read-outs towards a complete and efficient prediction of drug efficacy (Box1 – Levels III & IV). Thus profiling of PTGIS following 5Aza-dC and TSA treatments predicted residual cycling PTGIS^{pos} CSCs as being likely to regenerate a drug resistant hierarchy. Similarly, residual MEST^{neg} CSCs and all progenitors possibly contribute to curcumin refractoriness, while CB1007 treatment was ineffective in eliminating RXRγ^{pos} CSCs and progenitors. Thus, reversal of biomarker expression by itself is not sufficiently predictive due to cross-talks with other drug resistance mechanisms and detailed functional assays and resolution intratumor heterogeneity are essential in validating the accuracy of such predictions. Stabilization of the cell cycle to restrict aneuploidy is a novel, important effect of 5Aza-dC. Its combination with platinum/taxol (that resensitize cycling tumor cells towards apoptosis; 49, 50) and also including a drug that targets the tumor regenerative hierarchy may thereby be evaluated. Further, such potential epigenetic biomarkers need to be validated in randomized controlled trials to assign predictive power for specific epigenetic drugs

Legends to figures

Fig.1. Identification of differentially methylated genes in SeOvCa progression a-i. Heat map representing differentially methylated genes in the A4 progression model; a-ii Starburst plots correlating DNA methylation and expression of differentially methylated genes in A4 progression (76 hypomethylated - upregulated; 31 hypermethylated - downregulated); b-i. Heat map representing TCGA DNA methylation data, samples were segregated grade-wise into two groups (Group 1 - Grade I & II, n=75, left panel; Group 2 - Grade III, n=484, right panel); b-ii. Starburst plots correlating DNA methylation and expression of differentially methylated genes in Group 1 and Group 2 TCGA samples; c-i,ii. Venn diagram representing hypo- and hyper-methylated genes common to comparative stages between the A4 model and TCGA samples. d. Heat map representation of differentially methylated genes specific to d-i. A4-P cells and Group 1 tumors, d-ii. A4-T cells and Group 2 tumors

Fig.2. Validation of differentially methylated genes during SeOvCa progression. a. Bisulfite genomic sequencing (BGS) of hypomethylated (*CYC1,POGK,MAL,MEST*) and

hypermethylated (*PTGIS,FBN1*,*PAPSS2*) genes in A4P and A4T cells. Predicted CpG islands in gene promoters are indicated above the BGS profile; methylated and unmethylated CpGs are indicated as black and white circles respectively; CpG islands marked * were validated through BGS; transcriptional start site (TSS) is indicated as an arrow; Ci,Cii,Ciii represent CpG islands 1,2,3 respectively; methylation index is indicated in numbers above each BGS profile; b. Graphical representation of MI of differentially methylated genes validated through BGS; c. mRNA expression analysis through qRT-PCR of hypomethylated–upregulated and hypermethylated-downregulated genes; * p≤0.05; ** p≤0.01; *** p ≤0.001

Fig.3a. Venn diagram for monovalent (K4,K9,K27), bivalent (K4-K9,K9-K27,K4-K27) and trivalent (K4-K9-K27) marks enriched on gene promoters; b. Gene expression levels in enriched genes, K4, K4-K9 and K4-K27 marks associate with expressed genes (black bars), while K9, K27, K9-K27 and K4-K9-K27 marks correlate with lower expression (grey bars); c. Representative expression heat maps of genes regulated exclusively by histone modifications in TCGA ovarian cancer samples; Validation of histone marks in A4 progression model of 14 of these genes at d. transcriptional level; e. ChIP- qPCR (* p≤0.05; ** p≤0.01; *** p ≤0.001).

Fig.4. Efficacies of epigenetic drugs on A4 cells a. Induction of apoptosis by 5-Aza-dC, TSA, Curcumin and LSD1i in A4-P & A4-T cells profiled for Annexin-V-FITC and PI; b. Post-treatment frequencies of residual tumor subpopulations based on regenerative tumor hierarchy (left panels), Ploidy (central panels), cell cycle phases (right panels) for b-i.5-Az-dC, b-ii.TSA, b-iii.Curcumin, b-iv.CBB1007; c. Functional evaluation of capability of sorted tumor sub-fractions in controls and 5-Aza-dC-treated A4 xenografts for, c-i. Spheroid formation, c-ii. Clonogenicity (adherent colonies), c-iii. Soft agar colony formation (non-adherent, *in vitro* tumorogenicity), c-iv. Cell migration/Wound healing; *p<0.05,**p< 0.01,***p<0.001

Fig.5a. Modulation of gene expression dysregulated by DNA and histone methylation following epigenetic drug treatment of *in vitro* (1) and *in vivo* (2); b-i. Representative FACS profiles indicating effects of 5-Aza-dC and TSA on PTGIS expression (A4T cells-upper panel, xenografts-lower panel); b-ii. Immunofluorescence staining for PTGIS at

Day 12 in A4 spheroids formed from 5-Aza-dC/TSA-treated A4T cells; c,d. Representative graphs of analyses in $PTGIS^{neg}$ and $PTGIS^{neg}$ tumor fractions (1-control, 2-5-aza-dC and 3- TSA) for, c-i. Frequency of CSC hierarchy components, c-ii. Cycling of individual fractions red, blue and black lines represent cell cycle arrest, active cycling and absent fractions respectively; d. Frequency of ploidy-based fractions, d-ii. Cycling of individual fractions; *p<0.05, **p< 0.01, ***p<0.001

Fig.6. Representative FACS profiles indicating effects of a-i. Curcumin (1-control, 2-Curcumin), b-i. CBB1007 (1-control, 2-CBB1007) on *MEST* and *RXRγ* expression respectively (A4T cells-upper panels, xenografts-lower panels), accompanying are immunofluorescence images in tumor spheroids that lack *MEST* and upregulate *RXRγ* expression in the respective treatments; a-ii, b-ii. Representative graphs indicating frequency of CSC hierarchy components in $marker^{neg}$ and $marker^{neg}$ tumor fractions; a-iii,b-iii. Cycling of individual fractions red, blue and black lines denote cell cycle arrest, active cycling and absent fractions respectively; a-iv,b-iv. Representative graphs indicating frequency of CSC hierarchy components ploidy-based fractions within $marker^{neg}$ and $marker^{neg}$ tumor fractions; a-v,b-v. Cycling of individual fractions; *p<0.05, **p< 0.01, ***p<0.001

Acknowledgments

We thank the Experimental Animal and Confocal Facilities at NCCS for providing research support. Technical assistance by Ms. Rutika Naik and Mr. Avinash Mali is gratefully acknowledged.

Grant Support

Research is funded by grants to SAB from the Department of Biotechnology, Government of India, New Delhi (BT/PR/11465/MED/30/145/2008 & BT/Indo-Aus/06/03/2011). AKS received a research fellowship from the Council of Scientific and Industrial Research, New Delhi, India.

Disclaimer

Publicly available TCGA and GEO datasets were used in this study and are referenced.

Authors' Contributions

Conception and design, development of methodology and study supervision: SAB; Computational analysis: NC; Acquisition, analysis and interpretation of data: AKS, SAB; Writing of the manuscript: AKS, SAB

References

1. Sharma S, Kelly TK, Jones PA. Epigenetics in cancer. Carcinogenesis. 2010;31(1):27-36.
2. Baylin SB, Jones PA. A decade of exploring the cancer epigenome - biological and translational implications. Nat Rev Cancer. 2011;11(10):726-734.
3. Antequera F. Structure, function and evolution of CpG island promoters. Cell Mol Life Sci. 2003;60(8):1647-1658.
4. Issa JP. CpG island methylator phenotype in cancer. Nat Rev Cancer. 2004;4(12):988-993.
5. Deaton AM, Bird A. CpG islands and the regulation of transcription. Genes Dev. 2011;25(10):1010-1022.
6. Feldmann A, Ivanek R, Murr R, Gaidatzis D, Burger L, Schubeler D. Transcription factor occupancy can mediate active turnover of DNA methylation at regulatory regions. PLoS Genet. 2013;9(12):e1003994.
7. Houshdaran S, Zelenko Z, Irwin JC, Giudice LC. Human endometrial DNA methylome is cycle-dependent and is associated with gene expression regulation. Mol Endocrinol. 2014;28(7):1118-1135.
8. Zhang Y, Reinberg D. Transcription regulation by histone methylation: interplay between different covalent modifications of the core histone tails. 2001.
9. Zhou X, Sun H, Ellen TP, Chen H, Costa M. Arsenite alters global histone H3 methylation. Carcinogenesis. 2008;29(9):1831-1836.
10. Bapat SA. Modulation of gene expression in ovarian cancer by active and repressive histone marks. Epigenomics. 2010;2(1):39-51.
11. Boros J, Arnoult N, Stroobant V, Collet JF, Decottignies A. Polycomb repressive complex 2 and H3K27me3 cooperate with H3K9 methylation to maintain heterochromatin protein 1alpha at chromatin. Mol Cell Biol. 2014;34(19):3662-3674.

12. Cohen I, Poreba E, Kamieniarz K, Schneider R. Histone Modifiers in Cancer: Friends or Foes? Genes Cancer. 2011;2:631-647.
13. Arrowsmith CH, Bountra C, Fish PV, Lee K, Schapira M. Epigenetic protein families: a new frontier for drug discovery. Nature Reviews Drug Discovery. 2012;11(5):384-400.
14. Thinnes CC, England KS, Kawamura A, Chowdhury R, Schofield CJ, Hopkinson RJ. Targeting histone lysine demethylases - Progress, challenges, and the future. Biochim Biophys Acta. 2014 ;1839(12):1416-32.
15. Hashimoto H, Vertino PM, Cheng X. Molecular coupling of DNA methylation and histone methylation. E[pigenomics. 2010; 2(5): 657-669.
16. Greenlee RT, Hill-Harmon MB, Murray T, Thun M. Cancer statistics, 2001. CA Cancer J Clin. 2001;51(1):15-36.
17. Siegel R, Ma J, Zou Z, Jemal A. Cancer statistics, 2014. CA Cancer J Clin. 2014;64(1):9-29.
18. Baylin SB, Herman JG. DNA hypermethylation in tumorigenesis: epigenetics joins genetics. Trends Genet. 2000;16(4):168-174.
19. Dai W, Teodoridis JM, Zeller C, Graham J, Hersey J, Flanagan JM, et al. Systematic CpG islands methylation profiling of genes in the wnt pathway in epithelial ovarian cancer identifies biomarkers of progression-free survival. Clin Cancer Res. 2011;17(12):4052-4062.
20. Lyu T, Jia N, Wang J, Yan X, Yu Y, Lu Z, et al. Expression and epigenetic regulation of angiogenesis-related factors during dormancy and recurrent growth of ovarian carcinoma. Epigenetics. 2013;8(12):1330-1346.
21. Flanagan JM, Wilhelm-Benartzi CS, Metcalf M, Kaye SB, Brown R. Association of somatic DNA methylation variability with progression-free survival and toxicity in ovarian cancer patients. Ann Oncol. 2013;24(11):2813-2818.
22. Keita M, Wang ZQ, Pelletier JF, Bachvarova M, Plante M, Gregoire J, et al. Global methylation profiling in serous ovarian cancer is indicative for distinct aberrant DNA methylation signatures associated with tumor aggressiveness and disease progression. Gynecol Oncol. 2013;128(2):356-363.
23. Bapat SA, Jin V, Berry N, Balch C, Sharma N, Kurrey N, et al. Multivalent epigenetic marks confer microenvironment-responsive epigenetic plasticity to ovarian cancer cells. Epigenetics. 2010;5(8):716-729.

24. Marsh DJ, Shah JS, Cole AJ. Histones and their modifications in ovarian cancer - drivers of disease and therapeutic targets. Front Oncol. 2014;4:144.
25. Bapat SA, Mali AM, Koppikar CB, Kurrey NK. Stem and progenitor-like cells contribute to the aggressive behavior of human epithelial ovarian cancer. Cancer Res. 2005;65(8):3025-3029.
26. Cancer Genome Atlas Research Network. Integrated genomic analyses of ovarian carcinoma. Nature. 2011;474(7353):609-615
27. Kusumbe AP, Bapat SA. Cancer stem cells and aneuploid populations within developing tumors are the major determinants of tumor dormancy. Cancer Res. 2009;69(24):9245-9253.
28. Naik RR, Singh AK, Mali AM, Khirade MF, Bapat SA. A tumor deconstruction platform identifies definitive end points in the evaluation of drug responses. Oncogene. 2015 Apr 27. doi: 10.1038/onc.2015.130. [Epub ahead of print] PMID:25915841.
29. Kalra RS, Bapat SA. Expression proteomics predicts loss of RXR-gamma during progression of epithelial ovarian cancer. PLoS One. 2013;8(8):e70398.
30. Wu W, Bi C, Credille KM, Manro JR, Peek VL, Donoho GP, et al. Inhibition of tumor growth and metastasis in non-small cell lung cancer by LY2801653, an inhibitor of several oncokinases, including MET. Clin Cancer Res. 2013;19(20):5699-5710.
31. Bapat SA, Krishnan A, Ghanate AD, Kusumbe AP, Kalra RS. Gene expression: protein interaction systems network modeling identifies transformation-associated molecules and pathways in ovarian cancer. Cancer Res. 2010;70(12):4809-4819.
32. Subramanian A, Tamayo P, Mootha VK, Mukherjee S, Ebert BL, Gillette MA, et al. Gene set enrichment analysis: a knowledge-based approach for interpreting genome-wide expression profiles. Proc Natl Acad Sci USA 2005;102:15545–15550.
33. Gardi NL, Deshpande TU, Kamble SC, Budhe SR, Bapat SA Discrete molecular classes of ovarian cancer suggestive of unique mechanisms of transformation and metastases. Clin Cancer Res 2014;20(1):87-99.
34. Zhao Y and Simon R. BRB array tools data archive for human cancer gene expression: a unique and efficient data sharing resource. Cancer Informatics 2008;6:9-15.

35. Noushmehr H, Weisenberger DJ, Diefes K, Phillips HS, Pujara K, Berman BP, et al. Identification of a CpG island methylator phenotype that defines a distinct subgroup of glioma. Cancer Cell 2010;17(5):510-522.
36. Li LC. Designing PCR primer for DNA methylation mapping. Methods Mol Biol. 2007;402:371-384.
37. Bock C, Reither S, Mikeska T, Paulsen M, Walter J, Lengauer T. BiQ Analyzer: visualization and quality control for DNA methylation data from bisulfite sequencing. Bioinformatics. 2005;21(21):4067-4068.
38. Kurrey NK, Jalgaonkar SP, Joglekar AV, Ghanate AD, Chaskar PD, Doiphode RY, et al. Snail and slug mediate radioresistance and chemoresistance by antagonizing p53-mediated apoptosis and acquiring a stem-like phenotype in ovarian cancer cells. Stem Cells. 2009;27(9):2059-2068.
39. Riclet R, Chendeb M, Vonesch JL, Koczan D, Thiesen HJ, Losson R, et al. Disruption of the interaction between transcriptional intermediary factor 1beta and heterochromatin protein 1 leads to a switch from DNA hyper- to hypomethylation and H3K9 to H3K27 trimethylation on the MEST promoter correlating with gene reactivation. Mol Biol Cell.2010;20(1):296-305.
40. Kalra RS, Bapat SA. Enhanced levels of double-strand DNA break repair proteins protect ovarian cancer cells against genotoxic stress-induced apoptosis. J Ovarian Res. 2013; 6(1):66.
41. Lee PS, Teaberry VS, Bland AE, Huang Z, Whitaker RS, Baba T, et al. Elevated MAL expression is accompanied by promoter hypomethylation and platinum resistance in epithelial ovarian cancer. Int J Cancer. 2010;126(6):1378-1389.
42. Zeller C, Dai W, Steele NL, Siddiq A, Walley AJ, Wilhelm-Benartzi CS, et al. Candidate DNA methylation drivers of acquired cisplatin resistance in ovarian cancer identified by methylome and expression profiling. Oncogene. 2012;31(42):4567-4576.
43. Li G, Fu D, Liang W, Fan L, Chen K, Shan L, et al. CYC1 silencing sensitizes osteosarcoma cells to trail-induced apoptosis. Cell Physiol Biochem. 2014; 34:2070-2080.
44. Bethge N, Lothe RA, Honne H, Andresen K, Troen G, Eknæs M, et al. Colorectal cancer DNA methylation marker panel validated with high performance in Non-Hodgkin lymphoma. Epigenetics. 2014; 9(3); 428-436.

45. Italiano A. Prognostic or Predictive? It's Time to Get Back to Definitions! JCO 2011;29(35): 4718-4724.
46. Brown R, Curry E, Magnani L, Wilhelm-Benartzi CS, Borley J. Poised epigenetic states and acquired drug resistance in cancer. Nat Rev Cancer. 2014;14(11):747-753.
47. Ying D, Batra J, Singh AK, Bapat S, Judith CA. Transforming the Future of Treatment for Ovarian Cancer. Clin Exp Pharmacol. 2014;4:157.
48. Easwaran H, Tsai HC, Baylin SB. Cancer epigenetics: tumor heterogeneity, plasticity of stem-like states, and drug resistance. Mol Cell. 2014;54(5):716-727.
49. Fang F, Balch C, Schilder J, Breen T, Zhang S, Shen C, et al. A phase 1 and pharmacodynamic study of decitabine in combination with carboplatin in patients with recurrent, platinum-resistant, epithelial ovarian cancer. Cancer.2010;116 (17):4043-4053.
50. Glasspool RM, Brown R, Gore ME, Rustin GJ, McNeish IA, Wilson RH. et al. A randomised, phase II trial of the DNA-hypomethylating agent 5-aza-2'-deoxycytidine (decitabine) in combination with carboplatin vs carboplatin alone in patients with recurrent, partially platinum-sensitive ovarian cancer. Br J Cancer. 2014;110(8):1923-1929

Author Manuscript Published OnlineFirst on June 30, 2015; DOI: 10.1158/1078-0432.CCR-15-0505
Author manuscripts have been peer reviewed and accepted for publication but have not yet been edited.

Fig. 1.

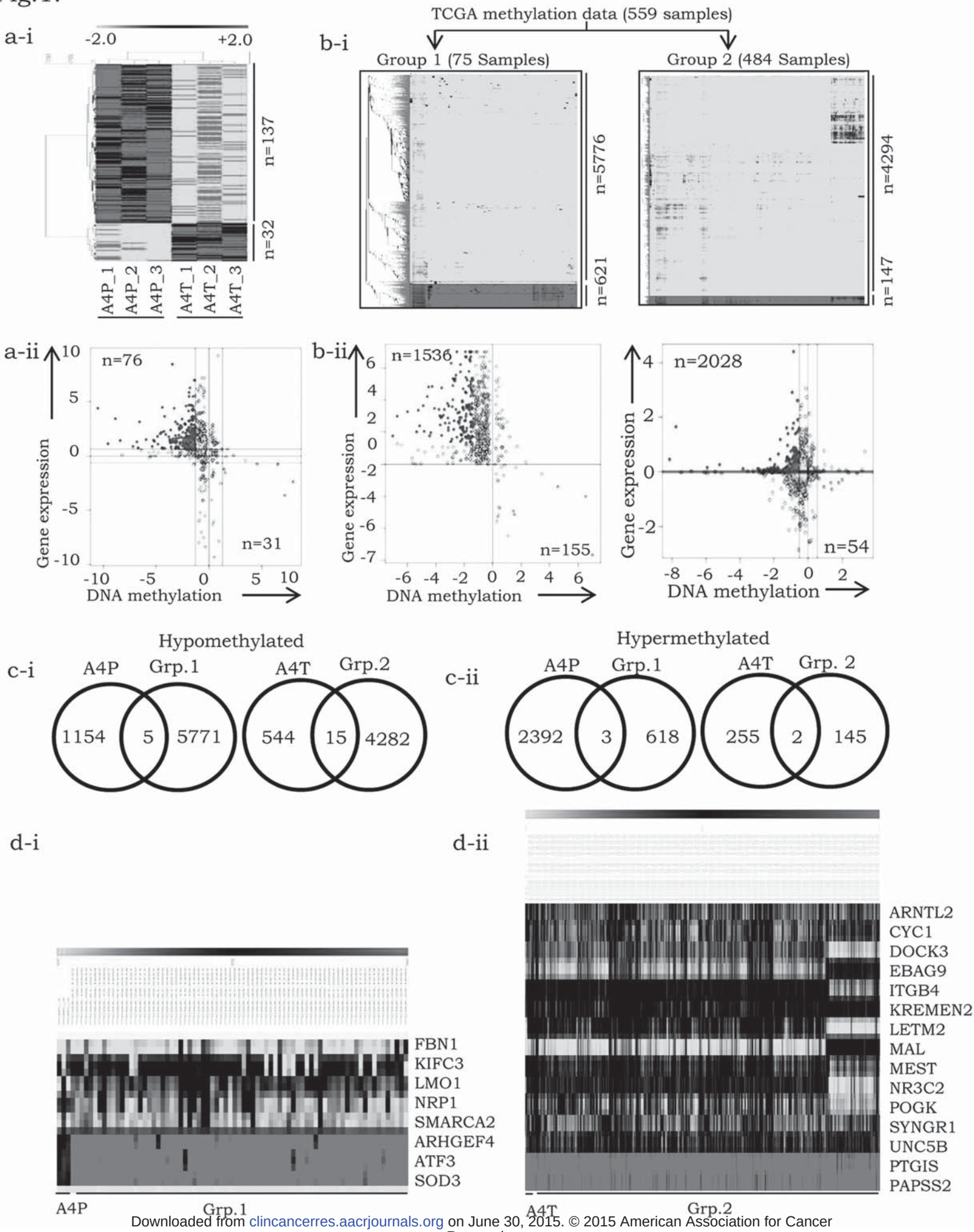

Fig. 2

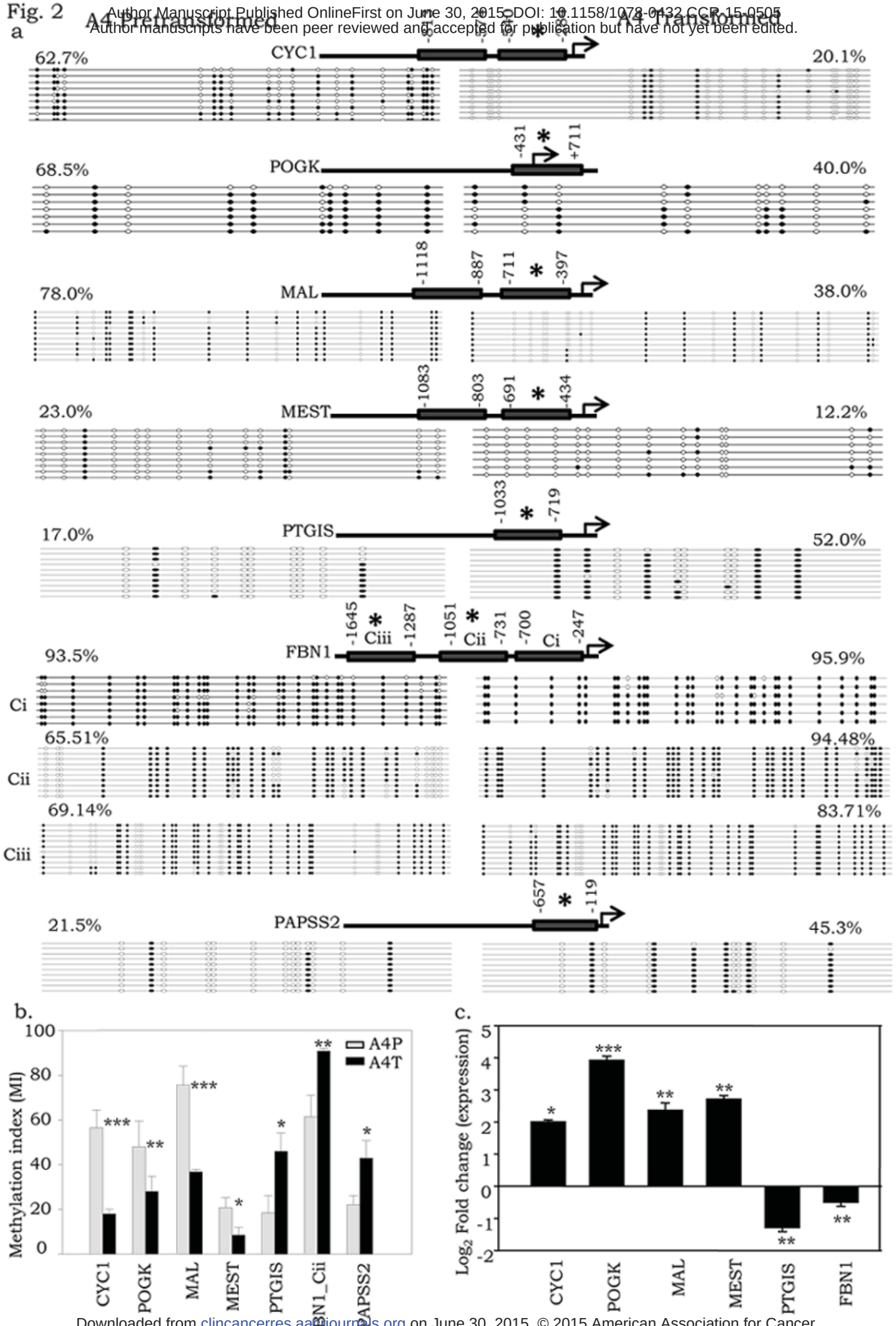

Fig. 3

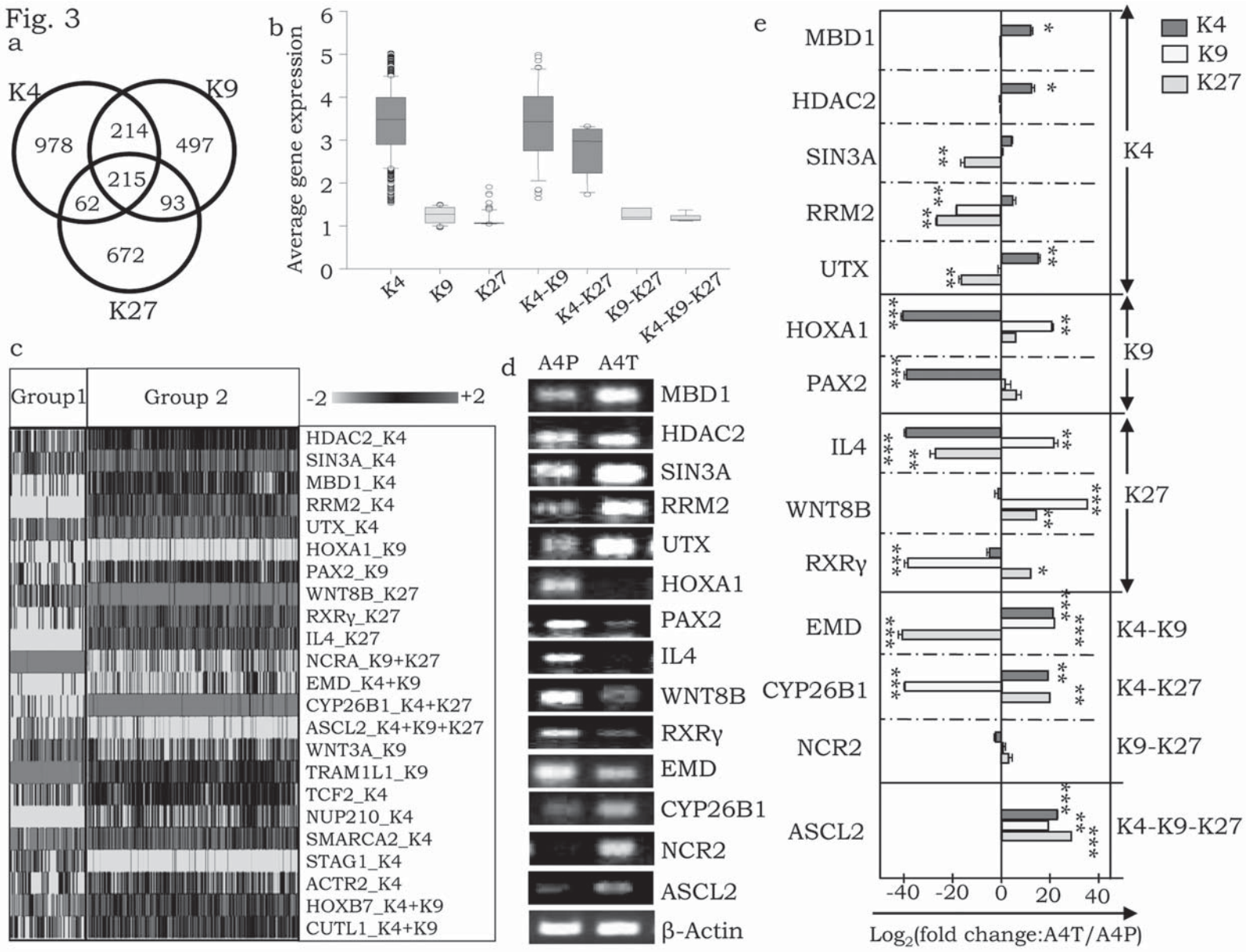

Author Manuscript Published OnlineFirst on June 30, 2015; DOI: 10.1158/1078-0432.CCR-15-0505
Author manuscripts have been peer reviewed and accepted for publication but have not yet been edited.

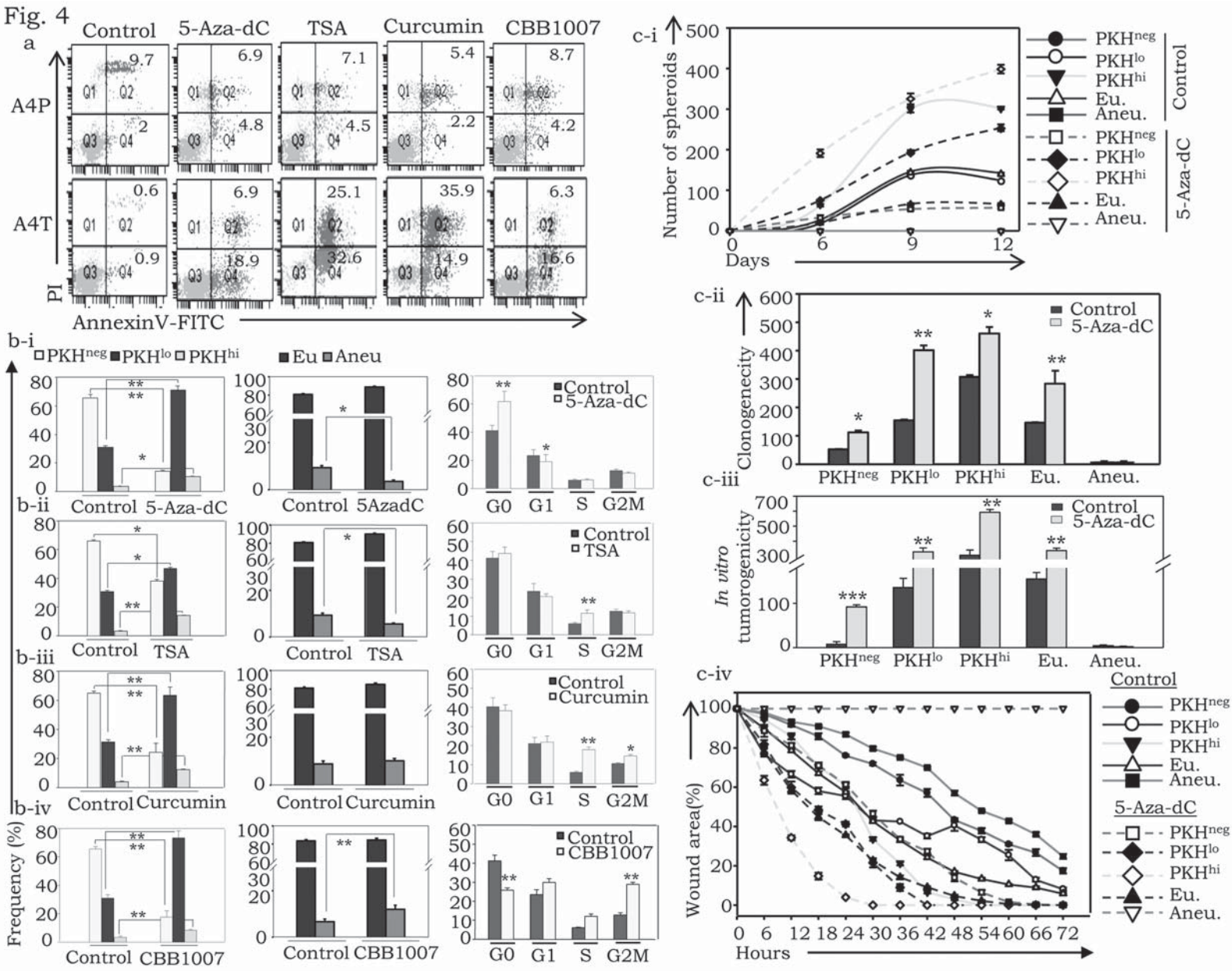

Author Manuscript Published OnlineFirst on June 30, 2015; DOI: 10.1158/1078-0432.CCR-15-0505
Author manuscripts have been peer reviewed and accepted for publication but have not yet been edited.

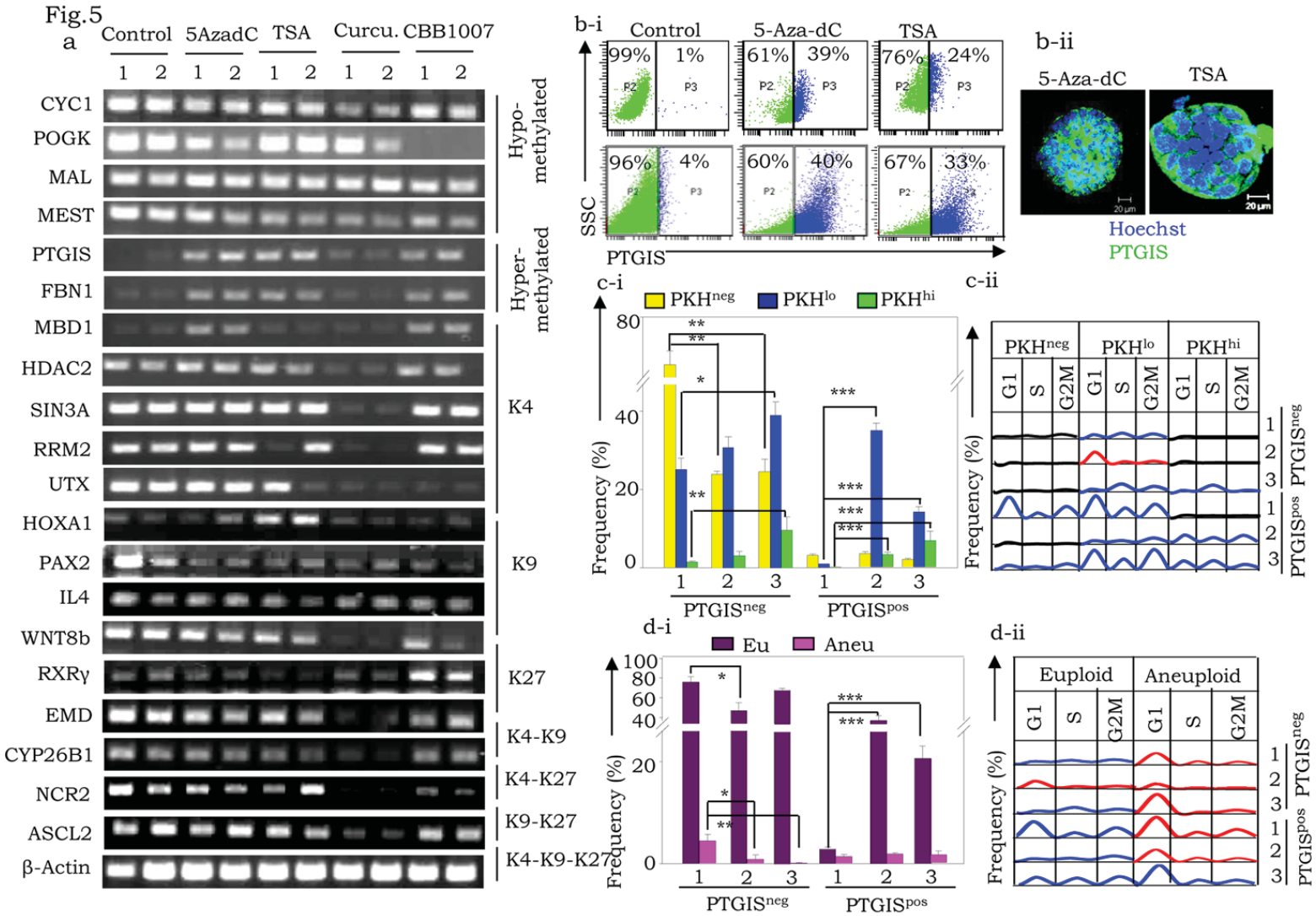

Fig.6

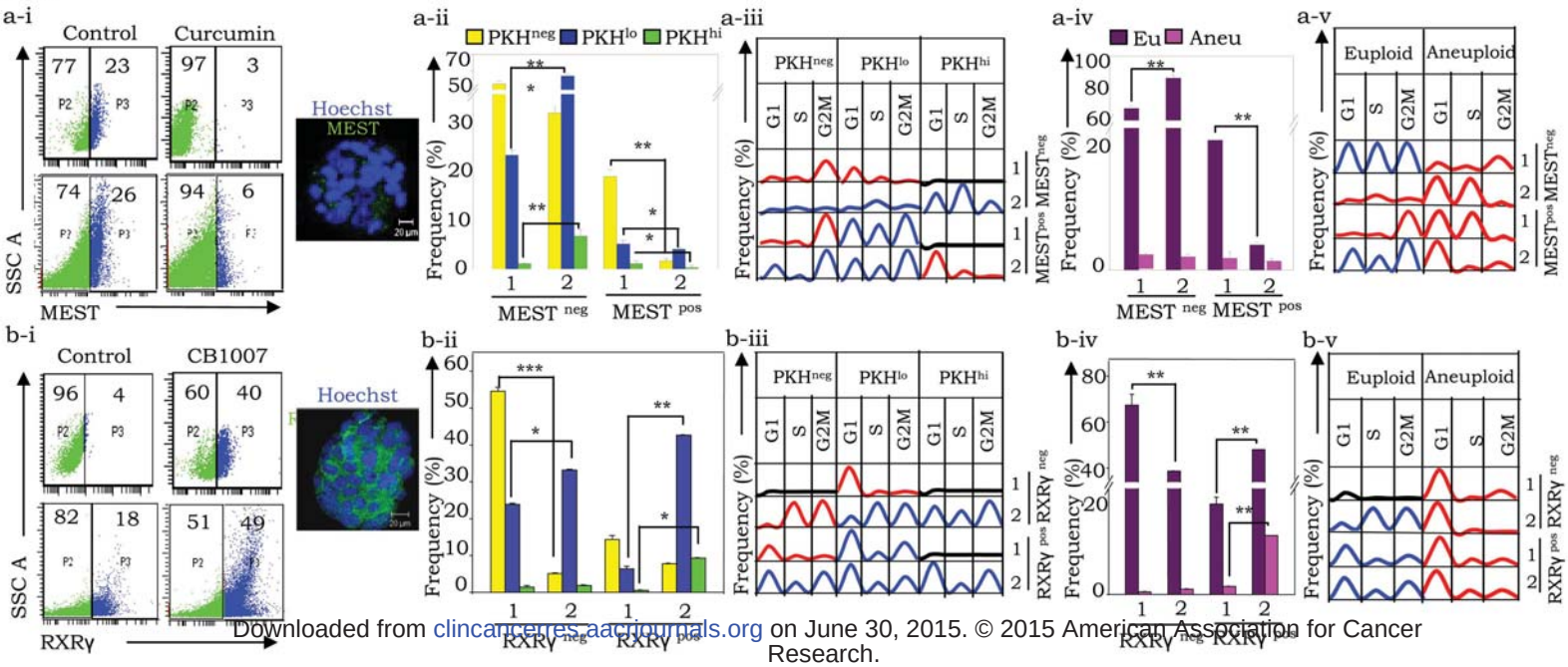

Author Manuscript Published OnlineFirst on June 30, 2015; DOI: 10.1158/1078-0432.CCR-15-0505
Author manuscripts have been peer reviewed and accepted for publication but have not yet been edited.

Box.1 Identification of potential biomarkers of response in epithelial ovarian cancer

I. Biomarker Identification and validation (Figs. 1,2,3; Supp. Figs. 1,2,3; Supp. Tables 1,2,3,4)

DNA methylation : 6 genes

Hypomethylated-upregulated - CYC1, MAL, MEST, POGK
Hypermethylated-downregulated: FBN1, PTGIS

Histone methylation : 14 genes

K4 - MBD1,HDAC2,SIN3A,RRM2,UTX
K9 - HOXA1,PAX2
K27 - IL4,WNT8B,RXRγ
K4-K9 - EMD
K4-K27 - CYP26B
K9-K27 - NCR2
K4-K9-K27 - ASCL2

II. Epigenetic Drug Screening (Figs.4,5a; Supp. Figs.4,5)

End-point	Assay	5-Aza-dC	TSA	Curcumin	CBB1007
Tumor Cell Cytotoxicity	(i) MTT (ii) Tumor regression (iii) Apoptosis (Annexin V)	√ √ √	√ √ √	√ √ √	√ √ √
Post-treatment regenerative potential	(i) PKH based hierarchy (ii) Spheroid formation	↑ CSCs ↓(1.5 fold)	↑ CSCs ↓(3 fold)	↑ CSCs ↓(2 fold)	↑ CSCs ↓(1.2 fold)
Genetic instability	DNA Content (Aneuploidy)	↓	↔	↔	↑
Cell cycle kinetics of residual cells	DNA & RNA Content	↑ G0	↑ S	↑ S	↑ G2M

III. Modulation of biomarker expression following treatment (Fig.5a; Supp. Figs.4,6a)

Drug	Biomarker	FACS quantification	
		Cultured cells	Tumor cells
5-Aza-dC	PTGIS	39 fold increase	10 fold increase
TSA	PTGIS	24 fold increase	8.25 fold increase
Curcumin	MEST	7.66 fold decrease	4 fold decrease
CBB1007	RXRγ	10 fold increase	2.7 fold increase

IV. Efficacy of drug treatment with respect to potential biomarker expression (Figs.6b,6c,6d; Supp.Figs.6b,6c,6d)

Drug	Biomarker	Effects following treatment
5-Aza-dC	PTGIS	(i) Diminished frequency of differentiated and aneuploid cells (ii) Drug resistance from self-renewing PTGIS^{pos} CSCs and progenitors
TSA	PTGIS	(i) Diminished frequency of differentiated and aneuploid cells (ii) Drug resistance from self-renewing residual PTGIS^{pos} CSCs and progenitors
Curcumin	MEST	(i) Diminished frequency of MEST^{pos} cells (ii) Enrichment of self-renewing MEST^{neg} CSCs and progenitors (iii) Induced cycling of MEST^{neg} aneuploid fractions
CBB1007	RXRγ	(i) Diminished frequency of RXRγ^{neg} differentiated fractions (ii) Drug resistance from self-renewing residual RXRγ^{pos} CSCs and aneuploid cells

AACR American Association for Cancer Research

Clinical Cancer Research

Evaluation of epigenetic drug targeting of heterogenous tumor cell fractions using potential biomarkers of response in ovarian cancer

Anand K Singh, Nishi Chandra and Sharmila A Bapat

Clin Cancer Res Published OnlineFirst June 30, 2015.